arXiv:cond-mat/0506667v1 [cond-mat.str-el] 24 Jun 2005

Spin dynamics of the quasi two dimensional spin-$\frac{1}{2}$ quantum magnet Cs_2CuCl_4

M. Y. Veillette, A. J. A. James and F. H. L. Essler
Rudolf Peierls Centre for Theoretical Physics,
University of Oxford, 1, Keble Road,
Oxford, OX1 3NP, United Kingdom

(Dated: December 25, 2021)

We study dynamical properties of the anisotropic triangular quantum antiferromagnet Cs_2CuCl_4. Inelastic neutron scattering measurements have established that the dynamical spin correlations cannot be understood within a linear spin wave analysis. We go beyond linear spin wave theory by taking interactions between magnons into account in a $1/S$ expansion. We determine the dynamical structure factor and carry out extensive comparisons with experimental data. We find that compared to linear spin wave theory a significant fraction of the scattering intensity is shifted to higher energies and strong scattering continua are present. However, the $1/S$ expansion fails to account for the experimentally observed large quantum renormalization of the exchange energies.

PACS numbers: 75.10.Jm, 75.25.+z,75.30.Ds.,75.40.Gb

I. INTRODUCTION

The quasi two dimensional spin-1/2 quantum magnet Cs_2CuCl_4 has attracted much theoretical and experimental interest in recent years as a possible realization of a two dimensional quantum spin liquid.[1,2,3,4,5,6,7,8,9,10,11,12] This anisotropic triangular Heisenberg antiferromagnet is believed to be a promising candidate due to its small spin, quasi two dimensionality and geometrically frustrated spin interactions. Although Cs_2CuCl_4 exhibits conventional incommensurate long range magnetic order at low temperatures, neutron scattering measurements have revealed unusual features in the spin excitation spectrum. In particular, the dynamical correlations are found to be dominated by an extended scattering continuum over a relatively large window of energies. Several workers have interpreted this observation as a signature of deconfined, fractionalized spin-1/2 (spinon) excitations, characteristic of a spin liquid phase. In this line of approach, the observed broad scattering continuum is interpreted in terms of a two-spinon scattering continuum.[7,9,12]

However, a strong scattering continuum does not entail an underlying spin liquid phase. In fact, a conventional magnetically ordered phase with strong magnon interactions can exhibit a broad continuum due to multi magnon scattering processes. A previous examination of the inelastic neutron scattering data on Cs_2CuCl_4 was performed in the framework of linear spin wave (LSW) theory.[4] The latter predicts sharp single particle excitations and weak two magnon scattering continua, features which were argued to be in poor agreement with the data. Given that the magnetic properties derive from small $S = 1/2$ Cu spins, one would *a priori* expect magnon interactions to play an important role. In order to assess the applicability of a spin wave based scenario to Cs_2CuCl_4 it is therefore necessary to go beyond linear spin wave theory.

On a qualitative level the predictions of nonlinear spin wave theory are readily anticipated. By Goldstone's theorem the breaking of a continuous symmetry in a magnetically ordered state enforces the presence of single particle excitations at low energies. As a result of the aforementioned interactions, these magnons acquire a finite life time, which in turn leads to a finite line width in the dynamical structure factor. Furthermore, compared to linear spin wave theory, spectral weight is transferred to higher energies via multi magnon scattering processes. In the case of Cs_2CuCl_4 one may expect the presence of a strong scattering continuum in the ordered phase because (1) the low spin and the frustrated nature of the exchange interactions lead to a small ordered moment and strong quantum fluctuations around the ordered state; (2) the magnon interactions in non-collinear spin structures like the ones found in Cs_2CuCl_4 induce a coupling between transverse and longitudinal spin fluctuations. This interaction provides an additional mechanism for damping the spin waves and can enhance the strength of the scattering continuum.

There is evidence of low-energy spin wave modes in the inelastic neutron scattering data. Sharp peaks are also observed at high energies near special wave vectors where a putative spin wave dispersion is at a saddle-point. It is important to note that this spin wave dispersion is dramatically "renormalized" compared to the prediction of linear spin wave theory.[3,4]

A priori it appears that nonlinear spin wave theory could have the necessary ingredients to account for the spin correlations observed in Cs_2CuCl_4. The issue then is whether it is possible to achieve a *quantitative* description of the experiments in low orders of perturbation theory in the spin wave interactions.

In the present work we go beyond linear spin wave theory and include, within the framework of a $1/S$ expansion, the quantum fluctuations around the classical ground state. We then apply the results to the case $S = 1/2$, in which the formal expansion parameter becomes of order 1 and is therefore not small. We are motivated by the observation that spin wave theory gives a good description of physical properties of the square-lattice spin-$\frac{1}{2}$ Heisenberg Hamiltonian.[13,14,15] Indeed, higher order (in a $1/S$ expansion) corrections to linear spin wave theory were shown to be small in this case. Furthermore, taking these corrections into account in the calculation of static and dynamical properties leads to an improved agreement with the results of more sophisticated numerical

techniques.[16,17,18] Although a corresponding analysis is not available for the frustrated triangular antiferromagnet, perturbative expansions in $1/S$ have shown the renormalization due to quantum effects is relatively small.[19,20,21,22]

This paper is organized as follows. The spin Hamiltonian for Cs_2CuCl_4 is introduced in Sec. II. In Sec. III we determine the magnon Green's function in the framework of a large-S expansion. In Sec. IV we relate the experimentally measured dynamical correlation functions to the magnon Green's function. The results of our analysis and comparisons to the experimental data on Cs_2CuCl_4 are presented in Sec. V. We conclude with a summary of our results in Sec. VI.

II. SPIN MODEL

The full spin Hamiltonian of Cs_2CuCl_4 has been determined previously from measurements in high magnetic fields (see Ref. 3 for details). For our purposes it suffices to note that the magnetic Cu^{2+} ions form a triangular lattice with anisotropic exchange interactions. As shown in Fig. 1, the main exchange interaction $J = 0.374(5)$ meV is along the crystallographic b axis ("chain direction"). A weaker spin exchange $J' = 0.128(5)$ meV occurs along the zig-zag bonds. Finally, a Dzyaloshinskii-Moriya (DM) interaction[23,24] $D = 0.020(2)$ meV is present along the zig-zag bonds.

Denoting the spin-$\frac{1}{2}$ operators at the sites $\mathbf{R}$ by $\mathbf{S_R}$, the quasi two dimensional Hamiltonian takes the form

$$\mathcal{H} = \sum_{\mathbf{R}} J\mathbf{S_R}\cdot\mathbf{S_{R+\delta_1+\delta_2}} + J'\left(\mathbf{S_R}\cdot\mathbf{S_{R+\delta_1}} + \mathbf{S_R}\cdot\mathbf{S_{R+\delta_2}}\right) - (-1)^n\mathbf{D}\cdot\mathbf{S_R}\times\left(\mathbf{S_{R+\delta_1}} + \mathbf{S_{R+\delta_2}}\right). \quad (1)$$

Here the vectors $\delta_\mathbf{1}$ and $\delta_\mathbf{2}$ connecting neighboring sites are shown in Fig. 1. The vector $\mathbf{D} = (D, 0, 0)$ is associated with the oriented bond between the two coupled spins connected by $\delta_\mathbf{1}$ or $\delta_\mathbf{2}$ and n is a layer index. The factor $(-1)^n$ indicates that the interaction alternates between even and odd layers, which as a result can be considered to be inverted versions of one another. A weak interlayer interaction J'' is also present between neighboring layers. However, as J'' is quite small we neglect it in the following.

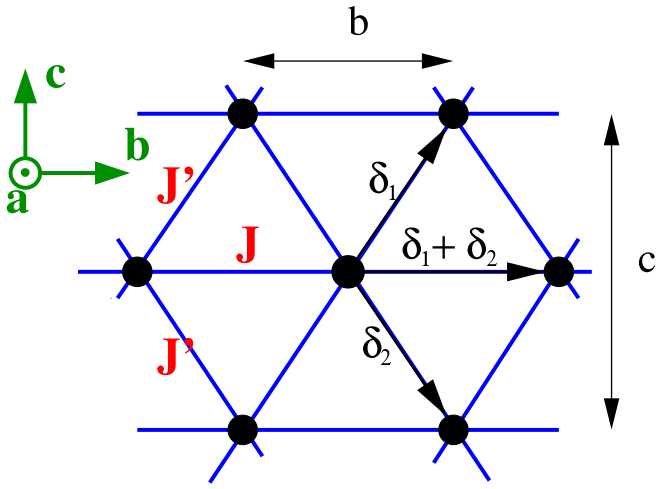


FIG. 1: (Color Online) The magnetic sites and exchange couplings within a single layer of Cs_2CuCl_4. Layers are stacked along the crystallographic a-direction with an interlayer spacing $a/2$ and a relative displacement in the c-direction.

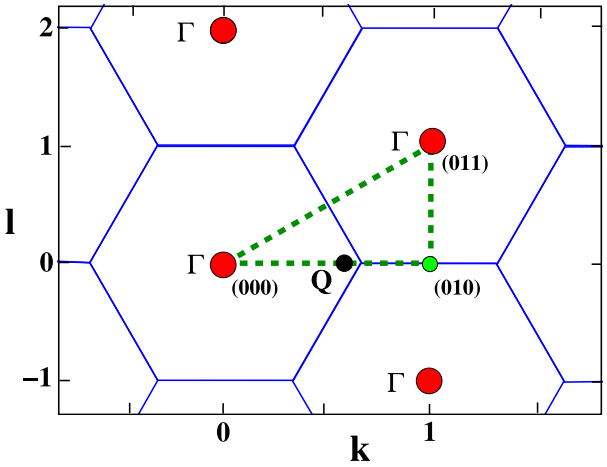


FIG. 2: (Color Online) The reciprocal space diagram of Cs_2CuCl_4 projected along the $(0, k, l)$ plane. The Γ points refer to the center of the Brillouin zone and $\mathbf{Q}$ is the ordering wave vector. The path of the cut shown in Fig. 3 is depicted as a dashed line.

Following the conventions of Coldea *et al.* in Ref. 4, we will discuss the dynamic response in terms of the two dimensional Brillouin zone of the triangular lattice even though the full crystal symmetry is orthorhombic. In our notation wave vectors are expressed in terms of the reciprocal lattice vectors as $\mathbf{k} = (h, k, l)$, which is a shorthand for $2\pi(h/a, k/b, l/c)$.

The Fourier transforms of the exchange and DM interactions are

$$J_\mathbf{Q} = J\cos(2\pi k) + 2J'\cos(\pi k)\cos(\pi l), \quad (2)$$

and

$$D_{\mathbf{Q}} = -2iD\sin(\pi k)\cos(\pi l). \quad (3)$$

It is convenient for what follows to define a quantity

$$J^T_{\mathbf{Q}} = J_{\mathbf{Q}} - iD_{\mathbf{Q}}. \quad (4)$$

Experimentally, spiral magnetic long range order is observed in Cs_2CuCl_4 at temperatures below $T_N = 0.62(1)K$. The ordered structure is found to lie in the bc plane by virtue of the small easy-plane anisotropy generated by the DM interactions. The spin structure is an incommensurate cycloid with an ordering wave vector $\mathbf{Q} = (0.0, 0.5 + \epsilon, 0)$ where $\epsilon = 0.030(2)$.

III. LARGE S EXPANSION

We now turn to a summary of our calculations. The procedure we follow is standard. We first express the fluctuations around the "classical" ground state in terms of boson operators using the Holstein-Primakoff transformation.[20,21,22,25,26,27,28,29] The term quadratic in the boson operators constitutes the basis for linear spin wave theory, whereas higher order terms represent spin wave interactions. The interaction vertices of n bosons carry a factor $S^{2-n/2}$, where S is the "length" of the spin. In the second step we determine the renormalized magnon Green's function by calculating the self-energy to leading order in $1/S$. Finally, the experimentally observable dynamical correlation functions are expressed in terms of the Green's function of the Holstein-Primakoff bosons.

The classical ground state is determined by treating the spins as classical vectors and then minimizing the energy. In this way one obtains a cycloidal structure with a characteristic wave vector $\mathbf{Q}$ that is fixed by the condition that it minimizes the exchange energy per spin, i.e. $J^T_{\mathbf{Q}} = \min_{\mathbf{q}} J^T_{\mathbf{q}}$. We find $\mathbf{Q} = (0.0, 0.5 + \epsilon_0, 0)$ with $\epsilon_0 = 0.054$. This value differs significantly from the measured incommensuration but quantum fluctuations lead to a reduction in ϵ_0 and taking them into account yields good agreement with experiments.[7,30]

As we have already indicated in Eq. (1), to a good approximation the layers are decoupled. Hence we consider from now on a set of independent 2-D layers, which are subdivided into two groups, differing according to the direction of the DM vector. For the case where the layer index n is odd (even), the DM vector is taken to point into (out of) the bc plane.

In what follows we present the results for the even layers only. However, it is easy to see that the spin structure factor is in fact independent of the layer index and the overall result is a simple summation over all layers.

It is convenient to define a local reference frame (x, y, z) such that the classical spin direction is aligned along the z axis at every site

$$\begin{pmatrix} S^a_{\mathbf{R}} \\ S^b_{\mathbf{R}} \\ S^c_{\mathbf{R}} \end{pmatrix} = \begin{pmatrix} 1 & 0 & 0 \\ 0 & \cos(\mathbf{Q}\cdot\mathbf{R}) & -\sin(\mathbf{Q}\cdot\mathbf{R}) \\ 0 & \sin(\mathbf{Q}\cdot\mathbf{R}) & \cos(\mathbf{Q}\cdot\mathbf{R}) \end{pmatrix} \begin{pmatrix} S^x_{\mathbf{R}} \\ S^y_{\mathbf{R}} \\ S^z_{\mathbf{R}} \end{pmatrix}. \quad (5)$$

The Holstein-Primakoff transformation reads[25]

$$\begin{aligned} S^+_{\mathbf{R}} &= S^x_{\mathbf{R}} + iS^y_{\mathbf{R}} = e^{i\theta}\sqrt{\left(2S - \phi^\dagger_{\mathbf{R}}\phi_{\mathbf{R}}\right)}\phi_{\mathbf{R}}, \\ S^-_{\mathbf{R}} &= S^x_{\mathbf{R}} - iS^y_{\mathbf{R}} = e^{-i\theta}\phi^\dagger_{\mathbf{R}}\sqrt{\left(2S - \phi^\dagger_{\mathbf{R}}\phi_{\mathbf{R}}\right)}, \\ S^z_{\mathbf{R}} &= S - \phi^\dagger_{\mathbf{R}}\phi_{\mathbf{R}}, \end{aligned} \quad (6)$$

where the boson creation and annihilation operators satisfy the canonical commutation relation $\left[\phi_{\mathbf{R}}, \phi^\dagger_{\mathbf{R}'}\right] = \delta_{\mathbf{R},\mathbf{R}'}$. Here θ is an arbitrary angle which we set equal to $\pi/2$ in order to make contact with the notation used in Ref. 21. Introducing the Fourier transform

$$\phi^\dagger_{\mathbf{k}} = \frac{1}{\sqrt{N}}\sum_{\mathbf{R}} \phi^\dagger_{\mathbf{R}} e^{-i\mathbf{k}\cdot\mathbf{R}}, \quad (7)$$

on a lattice of N sites, the Hamiltonian of Eq. (1) takes the form

$$\mathcal{H} = \mathcal{H}_0 + \mathcal{H}_2 + \mathcal{H}_3 + \mathcal{H}_4 + \cdots, \quad (8)$$

where $\mathcal{H}_n$ is proportional to $S^{2-n/2}$ and consists of normal ordered products of n boson operators. There is no $\mathcal{H}_1$ term, because Eq. (8) is an expansion around a minimum of the classical energy. Linear spin wave theory takes into account only the terms $\mathcal{H}_0$ and $\mathcal{H}_2$. The higher order terms represent interactions between magnons. The leading terms in the expansion are

$$\mathcal{H}_0 = NS^2 J^T_{\mathbf{Q}}, \tag{9}$$

$$\mathcal{H}_2 = NSJ^T_{\mathbf{Q}} + S\sum_{\mathbf{k}} A_{\mathbf{k}} \left(\phi^\dagger_{\mathbf{k}}\phi_{\mathbf{k}} + \phi_{-\mathbf{k}}\phi^\dagger_{-\mathbf{k}}\right) - B_{\mathbf{k}} \left(\phi^\dagger_{-\mathbf{k}}\phi^\dagger_{\mathbf{k}} + \phi_{-\mathbf{k}}\phi_{\mathbf{k}}\right), \tag{10}$$

$$\mathcal{H}_3 = \frac{i}{2}\sqrt{\frac{S}{2N}} \sum_{\mathbf{1,2,3}} \delta_{\mathbf{1+2+3}} \left(C_{\mathbf{1}} + C_{\mathbf{2}}\right) \left(\phi^\dagger_{-\mathbf{3}}\phi_{\mathbf{2}}\phi_{\mathbf{1}} - \phi^\dagger_{\mathbf{1}}\phi^\dagger_{\mathbf{2}}\phi_{-\mathbf{3}}\right), \tag{11}$$

$$\begin{aligned}\mathcal{H}_4 = \frac{1}{4N} \sum_{\mathbf{1,2,3,4}} \delta_{\mathbf{1+2+3+4}} \Big\{ &\frac{2}{3}\left(B_{\mathbf{2}} + B_{\mathbf{3}} + B_{\mathbf{4}}\right) \left(\phi^\dagger_{\mathbf{1}}\phi_{-\mathbf{2}}\phi_{-\mathbf{3}}\phi_{-\mathbf{4}} + \phi^\dagger_{-\mathbf{4}}\phi^\dagger_{-\mathbf{3}}\phi^\dagger_{-\mathbf{2}}\phi_{\mathbf{1}}\right) \\ + &\left[\left(A_{\mathbf{1+3}} + A_{\mathbf{1+4}} + A_{\mathbf{2+3}} + A_{\mathbf{2+4}}\right) - \left(B_{\mathbf{1+3}} + B_{\mathbf{1+4}} + B_{\mathbf{2+3}} + B_{\mathbf{2+4}}\right) - \left(A_{\mathbf{1}} + A_{\mathbf{2}} + A_{\mathbf{3}} + A_{\mathbf{4}}\right)\right] \phi^\dagger_{\mathbf{1}}\phi^\dagger_{\mathbf{2}}\phi_{-\mathbf{3}}\phi_{-\mathbf{4}} \Big\}\end{aligned} \tag{12}$$

Here the sum over $\mathbf{k}$ is performed in the first Brillouin zone and the subscripts $\mathbf{1}\ldots\mathbf{4}$ denote $\mathbf{k_1}\ldots\mathbf{k_4}$. The quantities $A_{\mathbf{k}}, B_{\mathbf{k}}$ and $C_{\mathbf{k}}$ are expressed as

$$\begin{aligned} A_{\mathbf{k}} &= \frac{1}{4}\left(2J_{\mathbf{k}} + J^T_{\mathbf{Q+k}} + J^T_{\mathbf{Q-k}}\right) - J^T_{\mathbf{Q}}, \\ B_{\mathbf{k}} &= \frac{1}{4}\left(2J_{\mathbf{k}} - J^T_{\mathbf{Q+k}} - J^T_{\mathbf{Q-k}}\right), \\ C_{\mathbf{k}} &= J^T_{\mathbf{Q+k}} - J^T_{\mathbf{Q-k}}. \end{aligned} \tag{13}$$

The coefficients $A_{\mathbf{k}}$ and $B_{\mathbf{k}}$ are even functions of $\mathbf{k}$, whereas $C_{\mathbf{k}}$ is an odd function of $\mathbf{k}$. In the absence of easy-plane anisotropies, i.e when D vanishes and inversion symmetry is present, we recover the results of Ref. 21. [Note that our definitions in Eqs. (13) differ from those of Ref. 21 by a factor of four.] We emphasize that the cubic interaction is generated as a result of the coupling between transverse and longitudinal fluctuations and hence can only exist in non-collinear spin structures. Furthermore, we note that the vertex factor $C_{\mathbf{k}} \propto |\mathbf{k}|^3$ for small $\mathbf{k}$ owing to the fact that $J^T_{\mathbf{Q}}$ is at a minimum by construction.

The quadratic Hamiltonian $\mathcal{H}_2$ is diagonalized by a Bogoliubov transformation

$$\begin{aligned} \phi_{\mathbf{k}} &= u_{\mathbf{k}}\gamma_{\mathbf{k}} + v_{\mathbf{k}}\gamma^\dagger_{-\mathbf{k}}, \\ \phi^\dagger_{-\mathbf{k}} &= v_{\mathbf{k}}\gamma_{\mathbf{k}} + u_{\mathbf{k}}\gamma^\dagger_{-\mathbf{k}}, \end{aligned} \tag{14}$$

where

$$\begin{aligned} u^2_{\mathbf{k}} &= 1 + v^2_{\mathbf{k}} = \frac{1}{2}\left(\frac{A_{\mathbf{k}}}{\sqrt{A^2_{\mathbf{k}} - B^2_{\mathbf{k}}}} + 1\right), \\ u_{\mathbf{k}}v_{\mathbf{k}} &= \frac{1}{2}\frac{B_{\mathbf{k}}}{\sqrt{A^2_{\mathbf{k}} - B^2_{\mathbf{k}}}}. \end{aligned} \tag{15}$$

The diagonal form of the quadratic Hamiltonian is

$$\mathcal{H}_2 = NSJ^T_{\mathbf{Q}} + \sum_{\mathbf{k}} \omega_{\mathbf{k}} \left(\gamma^\dagger_{\mathbf{k}}\gamma_{\mathbf{k}} + \frac{1}{2}\right), \tag{16}$$

where $\omega_{\mathbf{k}} = 2S\sqrt{A^2_{\mathbf{k}} - B^2_{\mathbf{k}}}$ is the linear spin wave dispersion relation.[26,27] We note that $\omega_{\mathbf{k}}$ is an even function of $\mathbf{k}$, despite the absence of inversion symmetry in the Hamiltonian. In fact, the symmetry of $\omega_{\mathbf{k}}$ is a consequence of time-reversal symmetry, which implies the following relation between the elements of the dynamical structure factor (Eq. 27),[31]

$$S^{\mu\nu}_{\mathbf{k},\omega} = S^{\nu\mu}_{-\mathbf{k},\omega}. \tag{17}$$

The importance of quantum fluctuations can be gauged by determining the average value of the local spin given by the standard formula

$$\langle S^z_{\mathbf{R}}\rangle = S - \Delta S = S - \frac{1}{2N}\sum_{\mathbf{k}} u^2_{\mathbf{k}} + v^2_{\mathbf{k}}. \tag{18}$$

The boson Green's function at zero temperature is expressed as

$$G_{\mathbf{k},\omega} = -i\int_{-\infty}^{\infty} dt e^{i\omega t} \left\langle T \begin{bmatrix} \phi_{\mathbf{k}}(t) \\ \phi^\dagger_{-\mathbf{k}}(t) \end{bmatrix} \begin{bmatrix} \phi^\dagger_{\mathbf{k}}(0)\phi_{-\mathbf{k}}(0) \end{bmatrix} \right\rangle, \tag{19}$$

where T denotes time ordering and $\langle ... \rangle$ represents a ground state expectation value. The inverse of the unperturbed Green's function is given by a 2×2 matrix,

$$G^{(0)-1}_{\mathbf{k},\omega} = (-2SA_{\mathbf{k}} + i\eta)\sigma^0 + 2SB_{\mathbf{k}}\sigma^x + \omega\sigma^z. \tag{20}$$

Here σ^0 and $\boldsymbol{\sigma}$ denote the identity and Pauli matrices respectively and $\eta = 0^+$.

The self-energy is defined by the Dyson equation,

$$G^{-1}_{\mathbf{k},\omega} = G^{(0)-1}_{\mathbf{k},\omega} - \Sigma_{\mathbf{k},\omega}, \tag{21}$$

and can be parameterized as

$$\Sigma_{\mathbf{k},\omega} = O_{\mathbf{k},\omega}\sigma^0 + X_{\mathbf{k},\omega}\sigma^x + Z_{\mathbf{k},\omega}\sigma^z. \tag{22}$$

The leading order (in $1/S$) contributions to the self-energy can be divided into two parts

$$\Sigma_{\mathbf{k},\omega} = \Sigma^{(4)}_{\mathbf{k}} + \Sigma^{(3)}_{\mathbf{k},\omega}. \tag{23}$$

Here $\Sigma^{(4)}_{\mathbf{k}}$ denotes the vacuum polarization contribution that arises in first order perturbation theory in $\mathcal{H}_4$. It is frequency independent and purely real. On the other hand, $\Sigma^{(3)}_{\mathbf{k},\omega}$

denotes the contribution in second order perturbation theory of the three-magnon interaction $\mathcal{H}_3$. It incorporates the effects of magnon decay. Using Eq. (20), the $\Sigma^{(4)}_{\mathbf{k}}$ contribution to the self-energy is found to be of the form

$$\begin{aligned} O^{(4)}_{\mathbf{k}} &= A_{\mathbf{k}} + \frac{2S}{N}\sum_{\mathbf{k}'}\frac{1}{\omega_{\mathbf{k}'}}\Big[\left(\frac{1}{2}B_{\mathbf{k}}+B_{\mathbf{k}'}\right)B_{\mathbf{k}'} \\ &+ \left(A_{\mathbf{k}-\mathbf{k}'}-B_{\mathbf{k}-\mathbf{k}'}-A_{\mathbf{k}'}-A_{\mathbf{k}}\right)A_{\mathbf{k}'}\Big], \\ X^{(4)}_{\mathbf{k}} &= -B_{\mathbf{k}} + \frac{2S}{N}\sum_{\mathbf{k}'}\frac{1}{\omega_{\mathbf{k}'}}\Big[\left(B_{\mathbf{k}}+B_{\mathbf{k}'}\right)A_{\mathbf{k}'} \\ &+ \left(A_{\mathbf{k}-\mathbf{k}'}-B_{\mathbf{k}-\mathbf{k}'}-A_{\mathbf{k}'}-\frac{1}{2}A_{\mathbf{k}}\right)B_{\mathbf{k}'}\Big], \\ Z^{(4)}_{\mathbf{k}} &= 0. \end{aligned} \tag{24}$$

The contribution $\Sigma^{(3)}$ is most easily evaluated in the Bogoliubov basis (γ) and is equal to

$$\begin{aligned} O^{(3)}_{\mathbf{k},\omega} &= \frac{-S}{16N}\sum_{\mathbf{k}'}\left\{\left[\Phi^{(1)}(\mathbf{k}',\mathbf{k}-\mathbf{k}')\right]^2+\left[\Phi^{(2)}(\mathbf{k}',\mathbf{k}-\mathbf{k}')\right]^2\right\}\left(\frac{1}{\omega_{\mathbf{k}'}+\omega_{\mathbf{k}-\mathbf{k}'}-\omega-i\eta}+\frac{1}{\omega_{\mathbf{k}'}+\omega_{\mathbf{k}-\mathbf{k}'}+\omega-i\eta}\right), \\ X^{(3)}_{\mathbf{k},\omega} &= \frac{-S}{16N}\sum_{\mathbf{k}'}\left\{\left[\Phi^{(1)}(\mathbf{k}',\mathbf{k}-\mathbf{k}')\right]^2-\left[\Phi^{(2)}(\mathbf{k}',\mathbf{k}-\mathbf{k}')\right]^2\right\}\left(\frac{1}{\omega_{\mathbf{k}'}+\omega_{\mathbf{k}-\mathbf{k}'}-\omega-i\eta}+\frac{1}{\omega_{\mathbf{k}'}+\omega_{\mathbf{k}-\mathbf{k}'}+\omega-i\eta}\right), \\ Z^{(3)}_{\mathbf{k},\omega} &= \frac{-S}{16N}\sum_{\mathbf{k}'}\left\{2\Phi^{(1)}(\mathbf{k}',\mathbf{k}-\mathbf{k}')\Phi^{(2)}(\mathbf{k}',\mathbf{k}-\mathbf{k}')\right\}\left(\frac{1}{\omega_{\mathbf{k}'}+\omega_{\mathbf{k}-\mathbf{k}'}-\omega-i\eta}-\frac{1}{\omega_{\mathbf{k}'}+\omega_{\mathbf{k}-\mathbf{k}'}+\omega-i\eta}\right), \end{aligned} \tag{25}$$

where

$$\begin{aligned} \Phi^{(1)}(\mathbf{k}',\mathbf{k}-\mathbf{k}') &= \left(C_{\mathbf{k}'}+C_{\mathbf{k}-\mathbf{k}'}\right)\left(u_{\mathbf{k}'}+v_{\mathbf{k}'}\right)\left(u_{\mathbf{k}-\mathbf{k}'}+v_{\mathbf{k}-\mathbf{k}'}\right)-2C_{\mathbf{k}}\left(u_{\mathbf{k}'}v_{\mathbf{k}-\mathbf{k}'}+v_{\mathbf{k}'}u_{\mathbf{k}-\mathbf{k}'}\right), \\ \Phi^{(2)}(\mathbf{k}',\mathbf{k}-\mathbf{k}') &= C_{\mathbf{k}'}\left(u_{\mathbf{k}'}+v_{\mathbf{k}'}\right)\left(u_{\mathbf{k}-\mathbf{k}'}-v_{\mathbf{k}-\mathbf{k}'}\right)+C_{\mathbf{k}-\mathbf{k}'}\left(u_{\mathbf{k}-\mathbf{k}'}+v_{\mathbf{k}-\mathbf{k}'}\right)\left(u_{\mathbf{k}'}-v_{\mathbf{k}'}\right). \end{aligned} \tag{26}$$

IV. DYNAMICAL CORRELATION FUNCTION

Inelastic neutron scattering experiments probe the dynamical structure factor $S^{\mu\nu}_{\mathbf{k},\omega}$. The latter is defined as the Fourier transform of the dynamical spin-spin correlation function

$$S^{\mu\nu}_{\mathbf{k},\omega} = \int_{-\infty}^{\infty}\frac{dt}{2\pi}e^{-i\omega t}\langle S^{\mu}_{-\mathbf{k}}(0)S^{\nu}_{\mathbf{k}}(t)\rangle. \tag{27}$$

Here $\mu,\nu=(a,b,c)$ label the various crystallographic axes and the Fourier-transformed spin operators are defined by $S^{\mu}_{\mathbf{k}}=\frac{1}{\sqrt{N}}\sum_{\mathbf{R}}S^{\mu}_{\mathbf{R}}e^{-i\mathbf{k}\cdot\mathbf{R}}$.

It is convenient to introduce time-ordered spin-spin correlation functions in the rotated coordinate system

$$F^{\alpha\beta}_{\mathbf{k},\omega} = -i\int_{-\infty}^{\infty}dt e^{-i\omega t}\langle TS^{\alpha}_{-\mathbf{k}}(0)S^{\beta}_{\mathbf{k}}(t)\rangle, \tag{28}$$

where $\alpha,\beta=(x,y,z)$ are the rotated coordinate axes (Eq. 5). The dynamical structure factor is related to the imaginary part of the time ordered correlation function in the following way

$$S^{aa}_{\mathbf{k},\omega} = -\frac{1}{\pi}\mathrm{Im}F^{xx}_{\mathbf{k},\omega}, \tag{29}$$

$$S^{bb}_{\mathbf{k},\omega} = S^{cc}_{\mathbf{k},\omega} = -\frac{1}{\pi}\mathrm{Im}\left[\Theta^{+}_{\mathbf{k}+\mathbf{Q},\omega}+\Theta^{-}_{\mathbf{k}-\mathbf{Q},\omega}\right], \tag{30}$$

$$S^{bc}_{\mathbf{k},\omega} = -S^{cb}_{\mathbf{k},\omega} = -\frac{i}{\pi}\mathrm{Im}\left[\Theta^{+}_{\mathbf{k}+\mathbf{Q},\omega}-\Theta^{-}_{\mathbf{k}-\mathbf{Q},\omega}\right], \tag{31}$$

where

$$\Theta^{\pm}_{\mathbf{k},\omega} = \frac{1}{4}\left[F^{zz}_{\mathbf{k},\omega}+F^{yy}_{\mathbf{k},\omega}\pm i\left(F^{zy}_{\mathbf{k},\omega}-F^{yz}_{\mathbf{k},\omega}\right)\right]. \tag{32}$$

To proceed further, we expand the dynamical correlation functions in inverse powers of S to order $\mathcal{O}(S^0)$. The corresponding results have been derived previously by Ohyama and Shiba.[21] Here we merely quote their results for the sake of completeness. The transverse correlations are

$$\begin{aligned} F^{xx}_{\mathbf{k},\omega} &= \frac{S}{2}c_x^2\mathrm{Tr}\left[\left(\sigma^0-\sigma^x\right)G_{\mathbf{k},\omega}\right], \\ F^{yy}_{\mathbf{k},\omega} &= \frac{S}{2}c_y^2\mathrm{Tr}\left[\left(\sigma^0+\sigma^x\right)G_{\mathbf{k},\omega}\right], \end{aligned} \tag{33}$$

where the Green's function is given by Eq. (21) and where

$$\begin{aligned} c_x &= 1-\frac{1}{4SN}\sum_{\mathbf{k}}\left(2v_{\mathbf{k}}^2-u_{\mathbf{k}}v_{\mathbf{k}}\right), \\ c_y &= 1-\frac{1}{4SN}\sum_{\mathbf{k}}\left(2v_{\mathbf{k}}^2+u_{\mathbf{k}}v_{\mathbf{k}}\right). \end{aligned} \tag{34}$$

We note that when squaring (34) only terms to order $\mathcal{O}(S^{-1})$ must be retained. The mixing of transverse and longitudinal fluctuations manifests itself in

$$\begin{aligned} i\left(F^{yz}_{\mathbf{k},\omega}-F^{zy}_{\mathbf{k},\omega}\right) = \quad & c_y\left\{P^{(1)}_{\mathbf{k},\omega}\mathrm{Tr}\left[\left(\sigma^0+\sigma^x\right)G_{\mathbf{k},\omega}\right]\right. \\ & \left.+\,P^{(2)}_{\mathbf{k},\omega}\mathrm{Tr}\left[\sigma^z G_{\mathbf{k},\omega}\right]\right\}. \end{aligned} \tag{35}$$

Here the functions $P^{(1,2)}_{\mathbf{k},\omega}$ are defined as

$$\begin{aligned} P^{(1)}_{\mathbf{k},\omega} &= \tfrac{S}{4N}\sum_{\mathbf{k}'}\Phi^{(1)}\left(\mathbf{k}',\mathbf{k}-\mathbf{k}'\right)\left(u_{\mathbf{k}'}v_{\mathbf{k}-\mathbf{k}'}+v_{\mathbf{k}'}u_{\mathbf{k}-\mathbf{k}'}\right)\left(\frac{1}{\omega_{\mathbf{k}'}+\omega_{\mathbf{k}-\mathbf{k}'}-\omega-i\eta}+\frac{1}{\omega_{\mathbf{k}'}+\omega_{\mathbf{k}-\mathbf{k}'}+\omega-i\eta}\right), \\ P^{(2)}_{\mathbf{k},\omega} &= \tfrac{S}{4N}\sum_{\mathbf{k}'}\Phi^{(2)}\left(\mathbf{k}',\mathbf{k}-\mathbf{k}'\right)\left(u_{\mathbf{k}'}v_{\mathbf{k}-\mathbf{k}'}+v_{\mathbf{k}'}u_{\mathbf{k}-\mathbf{k}'}\right)\left(\frac{1}{\omega_{\mathbf{k}'}+\omega_{\mathbf{k}-\mathbf{k}'}-\omega-i\eta}-\frac{1}{\omega_{\mathbf{k}'}+\omega_{\mathbf{k}-\mathbf{k}'}+\omega-i\eta}\right). \end{aligned} \tag{36}$$

Finally the longitudinal correlations are decomposed in inverse powers of S as $F^{zz}_{\mathbf{k},\omega}=F^{(0)zz}_{\mathbf{k},\omega}+F^{(1)zz}_{\mathbf{k},\omega}$, where

$$F^{(0)zz}_{\mathbf{k},\omega} = -\frac{1}{2N}\sum_{\mathbf{k}'}\left(u_{\mathbf{k}'}v_{\mathbf{k}-\mathbf{k}'}+v_{\mathbf{k}'}u_{\mathbf{k}-\mathbf{k}'}\right)^2\left(\frac{1}{\omega_{\mathbf{k}'}+\omega_{\mathbf{k}-\mathbf{k}'}-\omega-i\eta}+\frac{1}{\omega_{\mathbf{k}'}+\omega_{\mathbf{k}-\mathbf{k}'}+\omega-i\eta}\right), \tag{37}$$

$$F^{(1)zz}_{\mathbf{k},\omega} = \frac{1}{2S}\left\{\left(P^{(1)}_{\mathbf{k},\omega}\right)^2\mathrm{Tr}\left[\left(\sigma^0+\sigma^x\right)G_{\mathbf{k},\omega}\right]+\left(P^{(2)}_{\mathbf{k},\omega}\right)^2\mathrm{Tr}\left[\left(\sigma^0-\sigma^x\right)G_{\mathbf{k},\omega}\right]+2P^{(1)}_{\mathbf{k},\omega}P^{(2)}_{\mathbf{k},\omega}\mathrm{Tr}\left[\sigma^z G_{\mathbf{k},\omega}\right]\right\}. \tag{38}$$

We note that the $F^{(0)zz}$ term does not require the knowledge of the bosonic self-energy and is basically a free boson result. For this reason, it is often included in linear spin wave calculation as a source of two magnon scattering, even though it is formally a higher order contribution in $1/S$. In what follows, we abide by this (in some sense inconsistent) convention and consider the contribution of Eq. 37 as part of linear spin-wave theory. As a consequence we then retain the $F^{(1)zz}$ contribution to the dynamical structure factor, although of higher order in $1/S$ (i.e. $\mathcal{O}(S^{-1})$) than the other terms we take into account.

The (unpolarized) inelastic neutron scattering cross section is given by

$$\begin{aligned} \frac{d^2\sigma}{d\omega d\Omega} &= |f_{\mathbf{k}}|^2\sum_{\mu\nu}\left(\delta_{\mu\nu}-\hat{\mathbf{k}}_\mu\hat{\mathbf{k}}_\nu\right)S^{\mu\nu}_{\mathbf{k},\omega}, \\ &= |f_{\mathbf{k}}|^2\left[\left(1-\hat{\mathbf{k}}_a^2\right)S^{aa}_{\mathbf{k},\omega}+\left(1+\hat{\mathbf{k}}_a^2\right)S^{bb}_{\mathbf{k},\omega}\right], \end{aligned} \tag{39}$$

where $\hat{\mathbf{k}}_\mu$ is the μ-component of the unit vector in $\mathbf{k}$ direction. The magnetic form factor $f_{\mathbf{k}}$ is determined by the magnetic ions. For Cu^{2+}, the isotropic form factor has a relatively weak wave vector dependence within the first Brillouin zone and will be neglected from now on.[32]

It is well known that the $1/S$ expansion preserves many physical properties "order by order" in $1/S$. For instance, it follows from Eqs. (24, 25) that the Goldstone modes persist beyond linear spin wave theory as one expects on physical grounds. A careful examination also shows that to order $\mathcal{O}(S^0)$ the spectral functions are positive and that the relation (17) holds. However, due to a lack of self-consistency the $1/S$ expansion leads to an (unphysical) unequal treatment of the one-magnon and two magnon scattering contributions to dynamical correlation functions.[22] It is worthwhile to discuss this issue in more detail. The leading order contribution to the dynamical structure factor is due to coherent single magnon excitations and is of the form $\delta\left(\omega-\omega_{\mathbf{k}}\right)$. The two magnon contribution due to longitudinal fluctuations (Eq. 37) gives rise to a scattering continuum of the form $\sum_{\mathbf{k}'}I\left(\mathbf{k},\mathbf{k}'\right)\delta\left(\omega-\omega_{\mathbf{k}'}-\omega_{\mathbf{k}-\mathbf{k}'}\right)$ with some function $I\left(\mathbf{k},\mathbf{k}'\right)$. The extent of the two magnon contribution in $\mathbf{k}-\omega$ space is determined by the lower and upper bounds of the function $\omega_{\mathbf{k}'}+\omega_{\mathbf{k}-\mathbf{k}'}$ for a given $\mathbf{k}$.

On general grounds, we expect the lower bound of the two magnon scattering continuum to be equal to or smaller than the "true" magnon dispersion $\bar{\omega}_{\mathbf{k}}$. In fact, the existence of a zero-momentum Goldstone mode guarantees that there exists a two magnon contribution at frequencies $\bar{\omega}_{\mathbf{k}}+\bar{\omega}_{\mathbf{0}}=\bar{\omega}_{\mathbf{k}}$.

It is easy to see that this property does *not* hold order by order in a $1/S$ expansion. Indeed, the first order contribution in $1/S$ shifts the pole of the Green's function and leads to a renormalization of the magnon dispersion. The renormalized dispersion $\tilde{\omega}_{\mathbf{k}}$ can be determined from the Dyson equation

$$G^{-1}_{\mathbf{k},\tilde{\omega}_{\mathbf{k}}}=G^{(0)-1}_{\mathbf{k},\tilde{\omega}_{\mathbf{k}}}-\Sigma_{\mathbf{k},\tilde{\omega}_{\mathbf{k}}}=0. \tag{40}$$

However, to order $\mathcal{O}(S^0)$ the threshold of the two magnon contribution is still determined by the bare dispersion relation $\omega_{\mathbf{k}}$. This results in an unphysical behavior, where the two magnon scattering continuum is separated from the single

magnon dispersion by a gap. In order to avoid this problem, we impose the following self-consistency condition: *the linear spin wave dispersion $\omega_{\mathbf{k}}$ used in Eqs. (25, 36, 37) is to be replaced by the renormalized dispersion $\tilde{\omega}_{\mathbf{k}}$.*

V. DYNAMICAL PROPERTIES OF Cs_2CuCl_4

So far our discussion of the $1/S$ expansion has been fairly general. In order to make contact with the experiments on Cs_2CuCl_4 we now set the exchange constants to their appropriate values[3,4] and fix $S = 1/2$. We then evaluate the dynamical structure factor at a given wave vector numerically. Complex integrals such as Eqs. (25, 36) are evaluated by summing the imaginary part of the integrands over a frequency grid of 1200 points and of 1000×1000 points in wave vector space. The real parts are then determined from the Kramers-Kronig relations. The aforementioned self-consistency condition is implemented by calculating the full Green's function iteratively on a 100×100 grid in the Brillouin zone. We observe satisfactory numerical convergence after about three iterations.

We first turn to the magnon dispersion. The linear spin wave result $\omega_{\mathbf{k}}$ vanishes at the center of the paramagnetic Brillouin zone. The corresponding Goldstone mode is associated with small fluctuations of the ordered moment within the cycloidal plane. In helimagnets, the spectrum often exhibits a second Goldstone mode at the ordering wave vector. This gapless mode is due to fluctuations of the plane of the cycloid. In the case at hand, the easy-plane anisotropy generated by the DM term forces the cycloidal structure to lie in the bc plane and creates an excitation gap at the ordering wave vector $\mathbf{Q}$.

The renormalization of the magnon dispersion within the framework of the $1/S$ expansion is obtained from the poles of the Green's function (Eq. 40). In Fig. 4 we compare the results of the $1/S$ expansion with the linear spin wave theory. It is customary to quantify the effects of the "quantum" renormalization of the magnon dispersion by parametrizing the latter in terms of "effective" exchange constants $\tilde{J}, \tilde{J}', \tilde{D}$ and comparing them with the "bare" parameters J, J' and D.

Experimentally, the quantum renormalization is found to be rather large, namely $\frac{\tilde{J}}{J} = 1.63(5)$ and $\frac{\tilde{J}'}{J'} = 0.84(9)$. The renormalization of D was not established. The $1/S$ expansion yields the significantly smaller renormalizations $\frac{\tilde{J}}{J} = 1.131$, $\frac{\tilde{J}'}{J'} = 0.648$ and $\frac{\tilde{D}}{D} = 0.72$. The difference between the theoretical and experimental values indicates that the leading order in a $1/S$ expansion underestimates fluctuation effects. On the other hand one should note that the $1/S$ expansion gives a result of 0.031 for the incommensuration, which is very close to the experimentally observed value of $\epsilon = 0.030(2)$.

Before turning to a comparison of our results for the dynamical structure factor with the experimental results, we briefly review some facts about excitations in helimagnets. Generally it is useful to distinguish between three spin wave modes. In the case at hand, the "principal" mode $\omega^0_{\mathbf{k}} = \tilde{\omega}_{\mathbf{k}}$ is polarized along the a axis and is probed by the $S^{aa}_{\mathbf{k},\omega}$ component of the dynamical structure factor (Eq. 29). The two "secondary" spin wave modes $\omega^{\pm}_{\mathbf{k}} = \tilde{\omega}_{\mathbf{k}\pm\mathbf{Q}}$ are images of the main mode but their momenta are shifted by $\pm\mathbf{Q}$. They are polarized in the bc plane (Eqs. 30, 31). In linear spin wave theory, the three spin wave modes give rise to sharp δ functions and carry a large part of the spectral weight.

In addition to the single magnon modes there are multi magnon scattering continua. Whenever the magnon dispersion lies within a scattering continuum, the single magnon excitation gets broadened and acquires a finite line width. On the other hand, when the magnon dispersion lies at the threshold of a scattering continuum, there is no significant decay and the single magnon mode remains sharp.

The unpolarized dynamical structure factor (where the various polarizations are added according to Eq. 39) is shown in Fig. 3 as a function of energy and momentum for a particular "cut" of momentum transfers. The cut along the b direction, i.e. from (000) to (010), shows large modulations of the dispersion relation due to the strong intra-chain correlations. Near the ordering wave vector $\mathbf{Q}$ the scattering intensity increases sharply. For momentum transfers perpendicular to the chains, (i.e. along the (01η) direction), the single particle modes are seen to be resolution limited. The two in-plane modes become degenerate and their dispersions are nearly featureless, whereas the out-of-plane fluctuations dip to zero energy at (011), in accordance with Goldstone's theorem. Along the $(0\eta\eta)$ direction the spectrum is symmetric across the Brillouin zone boundary. Additional structures due to two magnon scattering are clearly visible at higher energies along the $(0\eta 0)$ and $(0\eta\eta)$ directions.

In order to illustrate how the spectral weights associated with the single-particle excitations are affected by the magnon interactions, we have estimated their contributions for each polarization to the integrated spectral weights. The total integrated intensity of each polarization is given by "equal-time" correlation functions,

$$\begin{aligned} I^0_{\mathbf{k}} &= -\frac{1}{\pi}\int d\omega\, F^{xx}_{\mathbf{k},\omega}, \\ I^{\pm}_{\mathbf{k}} &= -\frac{1}{\pi}\int d\omega\, \Theta^{\pm}_{\mathbf{k}\pm\mathbf{Q},\omega}. \end{aligned} \tag{41}$$

The one-magnon contribution to the integrated intensity of each polarization is then determined by integrating the respective correlation function in the vicinity of the single particle dispersions. In practice we find that integrating the peaks assuming a Lorentzian form is a poor prescription for strongly damped peaks. Instead we numerically integrate the intensity over an energy window of three times the width at half maximum

$$\begin{aligned} R^0_{\mathbf{k}} &= \frac{1}{I^0_{\mathbf{k}}}\int_{\omega^0_{\mathbf{k}}-1.5\Delta\omega^0_{\mathbf{k}}}^{\omega^0_{\mathbf{k}}+1.5\Delta\omega^0_{\mathbf{k}}} d\omega\, \frac{-F^{xx}_{\mathbf{k},\omega}}{\pi}, \\ R^{\pm}_{\mathbf{k}} &= \frac{1}{I^{\pm}_{\mathbf{k}}}\int_{\omega^{\pm}_{\mathbf{k}\pm\mathbf{Q}}-1.5\Delta\omega^{\pm}_{\mathbf{k}\pm\mathbf{Q}}}^{\omega^{\pm}_{\mathbf{k}\pm\mathbf{Q}}+1.5\Delta\omega^{\pm}_{\mathbf{k}\pm\mathbf{Q}}} d\omega\, \frac{-\Theta^{\pm}_{\mathbf{k}\pm\mathbf{Q},\omega}}{\pi}. \end{aligned} \tag{42}$$

The results are shown in Fig. 5. We see that the integrated spectral weight is concentrated in the vicinities of the ordering wave vector $\mathbf{Q}$ and $(0\frac{1}{2}\frac{1}{2})$ and is largely suppressed near

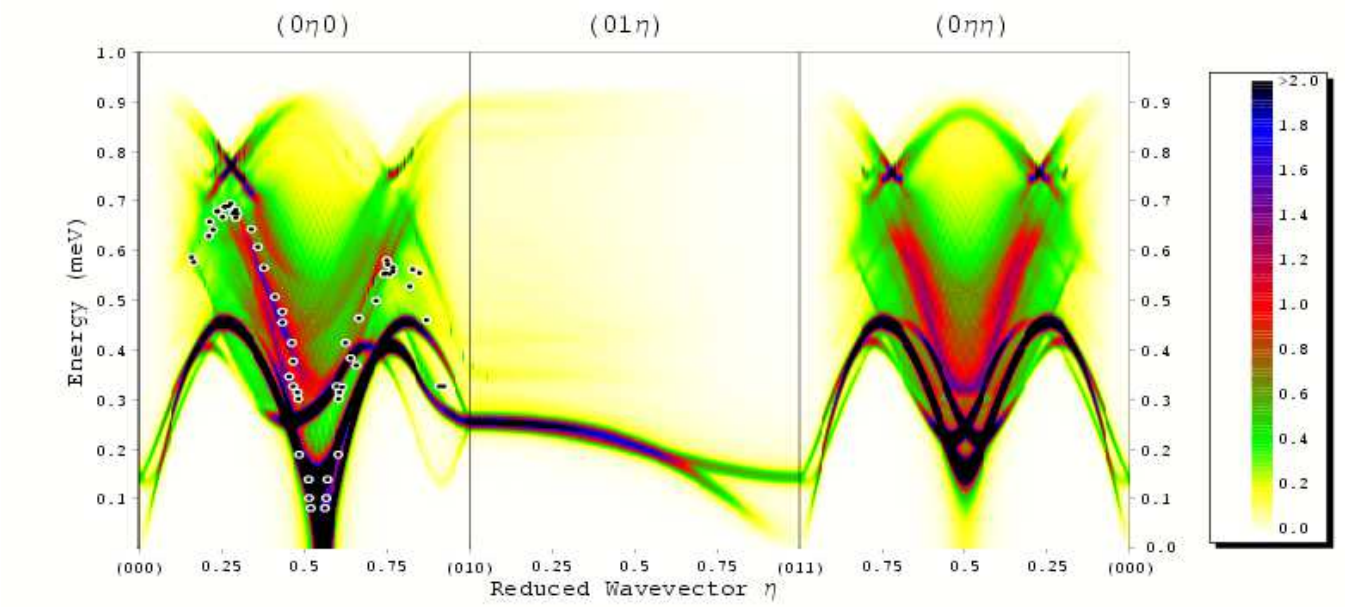


FIG. 3: (Color Online) Density plot of the scattering cross-section (Eq. 39) as a function of energy and wave vector. The light (dark) regions represent regions of small (large) scattering intensity. The results have been convolved with the experimental energy resolution of the detectors (The full width at half maximum is $\Delta E = 0.016$ meV). The magnetic form factor of copper in Eq. (39) shows very weak wave vector dependence in the regime of interest and therefore was taken to be unity.[32] The filled circles along the (010) direction are the experimental position of the most intense peaks in the line shapes taken in the spiral phase ($T < 0.1$K).[4]

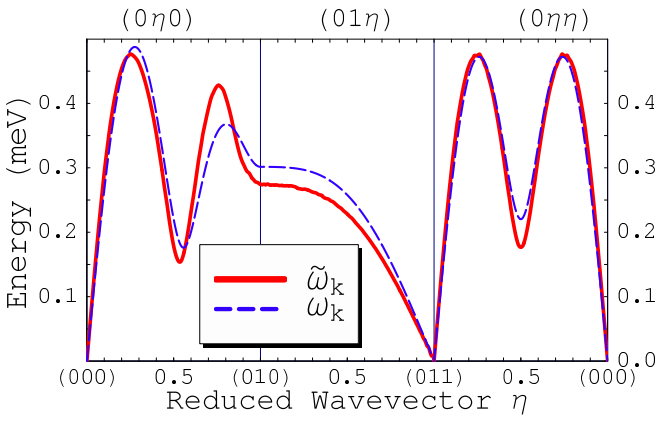


FIG. 4: (Color Online) The renormalization of the spin wave spectrum. The solid and dashed lines are results of the $1/S$ expansion $\tilde{\omega}_{\mathbf{k}}$ (Eq. 40) and the linear spin wave dispersion $\omega_{\mathbf{k}}$ (Eq. 16). The cut in the paramagnetic Brillouin zone runs from (000) to (010) to (011) and back to the center of the Brillouin zone (000).

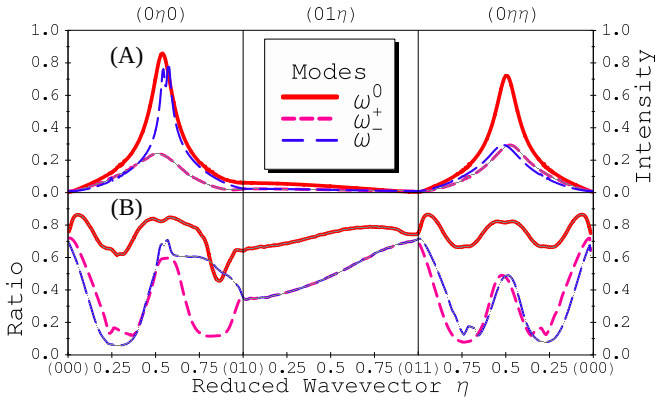


FIG. 5: (Color Online) Upper panel (A): The integrated spectral weights for the three polarizations (Eq. 41) as functions of momentum transfer. The principal ω^0 and secondary ω^+, ω^- spin wave modes are defined in the text. Lower panel (B): The ratios of the spectral weights of the single-particle excitations of each polarization to their respective integrated intensities (Eq. 42).

the Γ point. The weights associated with single magnon excitations are strongly suppressed for the secondary modes. This is a consequence of the non-collinearity of the magnetic order. The in-plane modes are significantly damped as a result of the coupling between longitudinal and transverse fluctuations. Such a coupling is not present for the out-of-plane mode and therefore the principal mode carries generally more spectral weight. Nevertheless the fraction of spectral weight associated with single-particle excitations decreases significantly whenever the renormalized spin wave dispersion is pushed upwards in energy for a given momentum. For instance, near wave vector $(0, 0.8, 0)$ the principal spin wave mode lies within the two magnon continuum and as a result less than 50 % of the spectral weight is attributed to the one-magnon excitation.

The scattering intensity can also be studied by performing a wave vector average,

$$I_T(\omega) = \frac{1}{N} \sum_{\mathbf{k}} \sum_{\mu} S^{\mu\mu}_{\mathbf{k},\omega}. \tag{43}$$

By the frequency sum rule, the scattering intensity (Eq. 43) integrated over all energies (including the elastic Bragg peaks at $\omega = 0$) has to equal $S(S+1)$. However, this sum rule does not hold "order by order" in perturbation theory. For instance, the total intensity within linear spin wave theory exceeds the sum rule by $\Delta S(1 + 2\Delta S)$. Bearing this caveat in mind, the sum rule is a useful tool for comparing the one and two magnon contributions as well as analyzing the shift in spectral weight. In Fig. V, we plot the scattering intensities as functions of energy within linear spin wave theory and the $1/S$ expansion. In linear spin wave theory the integrated intensity exhibits cusps, which are associated with van-Hove singularities in the single particle density of states. In the $1/S$ expansion such sharp features are absent. Above approximately 0.5 meV the one magnon contribution vanishes and the scattering intensity is entirely due to multi magnon states.

To quantify the shift of the spectral weight we calculate the first moment of the normalized scattering intensity $\langle\omega\rangle$. We find that the linear spin wave theory value $\langle\omega\rangle = 0.35$ meV is renormalized upwards to $\langle\omega\rangle = 0.40$ meV in the $1/S$ expansion. This observation is in line with the expectation that the higher orders of the $1/S$ expansion induce a transfer of spectral weight to higher energies via multi magnon scattering processes. In fact, as shown in Fig. V the two magnon contribution to the overall intensity is 29% in linear spin wave theory but 46% in the $1/S$ expansion.

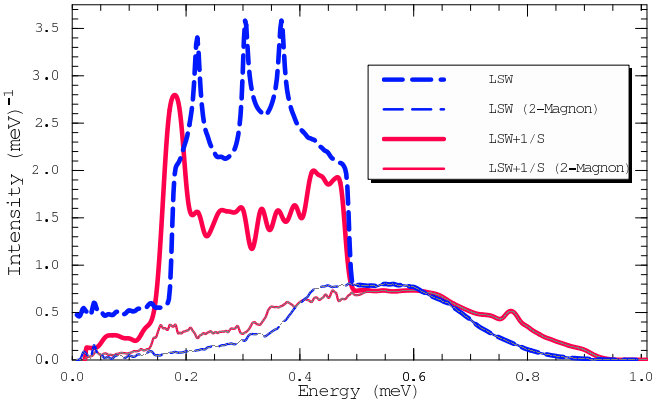


FIG. 6: (Color Online) The scattering intensity as a function of energy (Eq. 43) for LSW theory (dashed line) and LSW+1/S expansion (solid line). The contributions of the scattering continua is shown using thin lines.

A. Excitation line shapes

In order to exhibit the properties of the dynamical structure factor in greater detail we have generated a series of scans in $\mathbf{k}-\omega$ space. The inelastic neutron scattering measurements on Cs_2CuCl_4 were not performed at constant momentum transfer but followed various trajectories in energy-wave vector space. We have generated our theoretical scans using the known parameterizations of the scans A to J of Ref. 4 in $\mathbf{k}-\omega$ space, which we summarize in Table. I. We refer the reader to Ref. 4

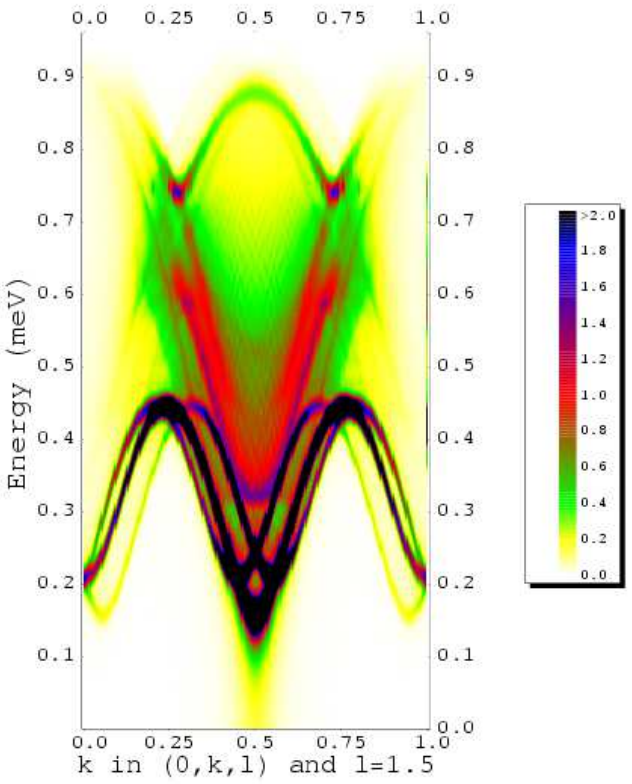


FIG. 7: (Color Online) Density plot of the scattering cross-section as a function of energy and wave vector along the cut $(0k\frac{3}{2})$. The light (dark) regions represent regions of small (large) scattering intensity.

for further details. The various scans are shown in Fig. 8. Also shown are the regions in which significant magnetic scattering is observed experimentally and the location of the main peaks. For comparison we plot the principal and secondary spin wave dispersions obtained from the $1/S$ expansion. As we have already emphasized, the $1/S$ expansion underestimates the quantum renormalization of the exchange constants and as a result the agreement of the calculated spin wave dispersions with the main peaks observed experimentally is poor.

The experimental energy and momentum resolutions have been accounted for to make contact with experiment. We find that the effects of the finite energy resolution of $\Delta E = 0.016$ meV are generally outweighed by the effects of the finite momentum resolution. This is a consequence of the large modulation of the spin wave dispersion along the chain direction, i.e $(0k0)$, (whose slopes can reach $\frac{\Delta E}{\Delta k} \sim 1.6$ meV), which causes an amplification of the effects of the momentum resolution. Given that the spin waves are nearly dispersionless along the $(00l)$ direction, we have only taken into account the spatial resolution along the chain direction.

To illustrate this point, let us consider the results for scans B, E, G and H shown in Fig. 9. The insets of panel (4) show the results of both linear spin wave theory and the $1/S$ expansion for a hypothetical energy resolution of $\Delta E = 0.002$ meV which has been introduced to make the various delta function peaks visible (the momentum resolution is set to zero

#	k(rlu)	l(rlu)	$\hat{\mathbf{k}}_a$
A	$-0.389+0.189E-0.016E^2$	0	0.05
B	$-0.30+0.189E-0.015E^2$	0	0.02
C	$0.21+0.297E-0.026E^2$	0	0.25
D	$2.11+0.29E-0.025E^2$	0	0.95
E	$-0.33+0.19E-0.015E^2$	$0.78+0.37E-0.03E^2$	1
F	$-0.39+0.19E-0.02E^2$	$1.66+0.37E-0.035E^2$	1
G	0.5	$1.53-0.32E-0.1E^2$	1
H	$0.28+0.29E-0.025E^2$	1.205	1
J	0.47	$1.0-0.45E$	1
K	$0.29+0.29E-0.03E^2$	$0.77-0.14E+0.013E^2$	1

TABLE I: Parameterization of energy-momentum scans performed in Ref. 4: the momentum transfers $\mathbf{k}=(h,k,l)$ are parameterized in terms of the energy transfer E (in meV). $\hat{\mathbf{k}}_a$ is a measure of the polarization factor. Given that the weak interlayer coupling is neglected, h is not needed for the purpose of our calculation.

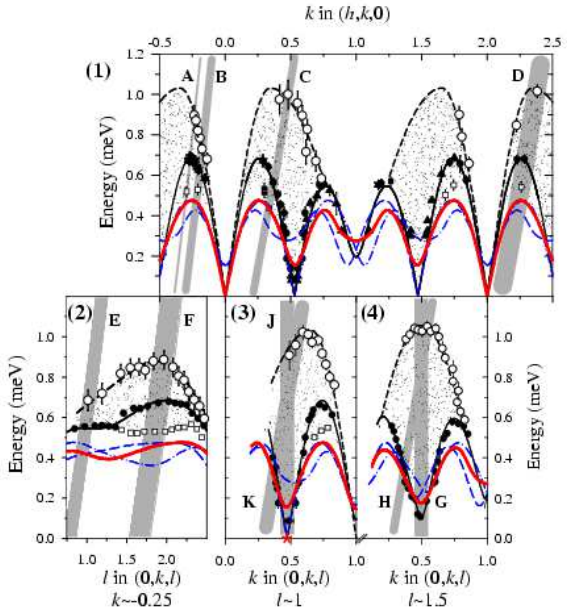


FIG. 8: (Color Online) The dispersion relation of magnetic excitations. The shaded regions labeled with capital letters A through K indicate scan directions (the line thickness indicates the wave vector averaging). The filled symbols are the main peaks in the line shape as determined experimentally in the ordered phase (from Ref. 4). The dotted area indicates the extent of the scattering continuum. The open circles and squares are respectively the upper and lower boundary of the scattering continuum as determined experimentally. The upper thick dashed line is a guide to the eye. The thin solid line is the experimental fit to the principal mode using effective parameters ($\tilde{J}=0.61$ meV, $\tilde{J}'=0.107$ meV). The thick solid, dashed and dash dotted lines are respectively the $1/S$ results for the principal ($\omega^0_{\mathbf{k}}$) and secondary ($\omega^+_{\mathbf{k}}$, $\omega^-_{\mathbf{k}}$) modes determined from Eq. 40.

$\Delta k=0$). First we consider the results for scan H (Panel 4 of Fig. 9). Linear spin wave theory predicts peaks at approximately 0.27 meV and 0.37 meV corresponding to the degenerate spin wave modes ω^+,ω^0 and to ω^- respectively. The $1/S$ correction yields a slight upward shift in the energy of these peaks. In both linear spin-wave and $1/S$ calculations, the two magnon scattering continuum is found to carry nearly a quarter of the integrated spectral weight. Taking into account the finite momentum resolution (the width at half maximum is $\Delta k=0.057$) we find that the sharp peaks get broadened very significantly as is shown in panel (4). The dynamical structure factor now exhibits an extended continuum in which the single-particle excitation can no longer be resolved and merges smoothly with the two magnon continuum. This result is qualitatively similar to the experimental observations shown for comparison in panel (2) of Fig. 10.

Next we turn to scan G (Panel 3 of Fig. 9), which probes the vicinity of the wave vector $(0,0.5,1.5)$. Experimentally a resolution-limited peak is observed at an energy of $0.107(10)$ meV in this region of intense scattering, see panel (1) of Fig.10. However, about two thirds of the spectral weight is associated with a scattering continuum at higher energies. Both linear spin wave theory and the $1/S$ expansion predict sharp peaks in this region of the Brillouin zone. The $1/S$ expansion gives a spin wave peak at $\omega^0=0.18$ meV carrying nearly half of the spectral weight and two further peaks at energies around 0.25 meV corresponding to the two secondary spin wave modes. The two magnon scattering continuum extends up to 0.9 meV and carries nearly a quarter of the spectral weight. We emphasize that, in contrast to $\omega^{\pm}$, the principal mode ω^0 is close to a saddle point and therefore is nearly dispersionless. In Panel 3 the finite energy and momentum resolutions are taken into account. We see that the almost dispersionless main mode remains sharp but the secondary modes can no longer be resolved and are found to merge with the two magnon continuum. Irrespective of the discrepancies between the results of the $1/S$ expansions and the experimental data, our calculation suggests that the lower boundary of of the measured scattering continuum in scan G could be due to unresolved transverse magnons. Such a scenario had been previously considered and ruled out on the basis of the smallness of the ratio $I_{\rm sec}/I_{\rm pri}$ of spectral weights of the secondary modes to the principal mode predicted by linear spin wave theory.[4] However, the results of the $1/S$ expansion show that spin wave interactions lead to an enhancement of this ratio for the G scan.

Next, we examine scan E (Panel 2), which probes wave vectors near $\mathbf{k}=(0,-0.25,1)$. Linear spin wave theory predicts coherent peaks at $\omega^0=0.35$ meV for the principal mode and at $\omega^-=0.44$ meV and $\omega^+=0.33$ meV for the secondary modes (see the inset in Panel 2). The two magnon scattering continuum is relatively weak and carries only about 23 % of the total spectral weight. In the framework of the $1/S$ expansion the principal mode is pushed upwards in energy to $\omega^0=0.42$ meV and occurs very close to the secondary mode $\omega^-=0.45$ meV. The other secondary mode ω^+ is shifted very significantly to 0.39 meV, but carries only a minute fraction of the spectral weight. The two magnon continuum is also

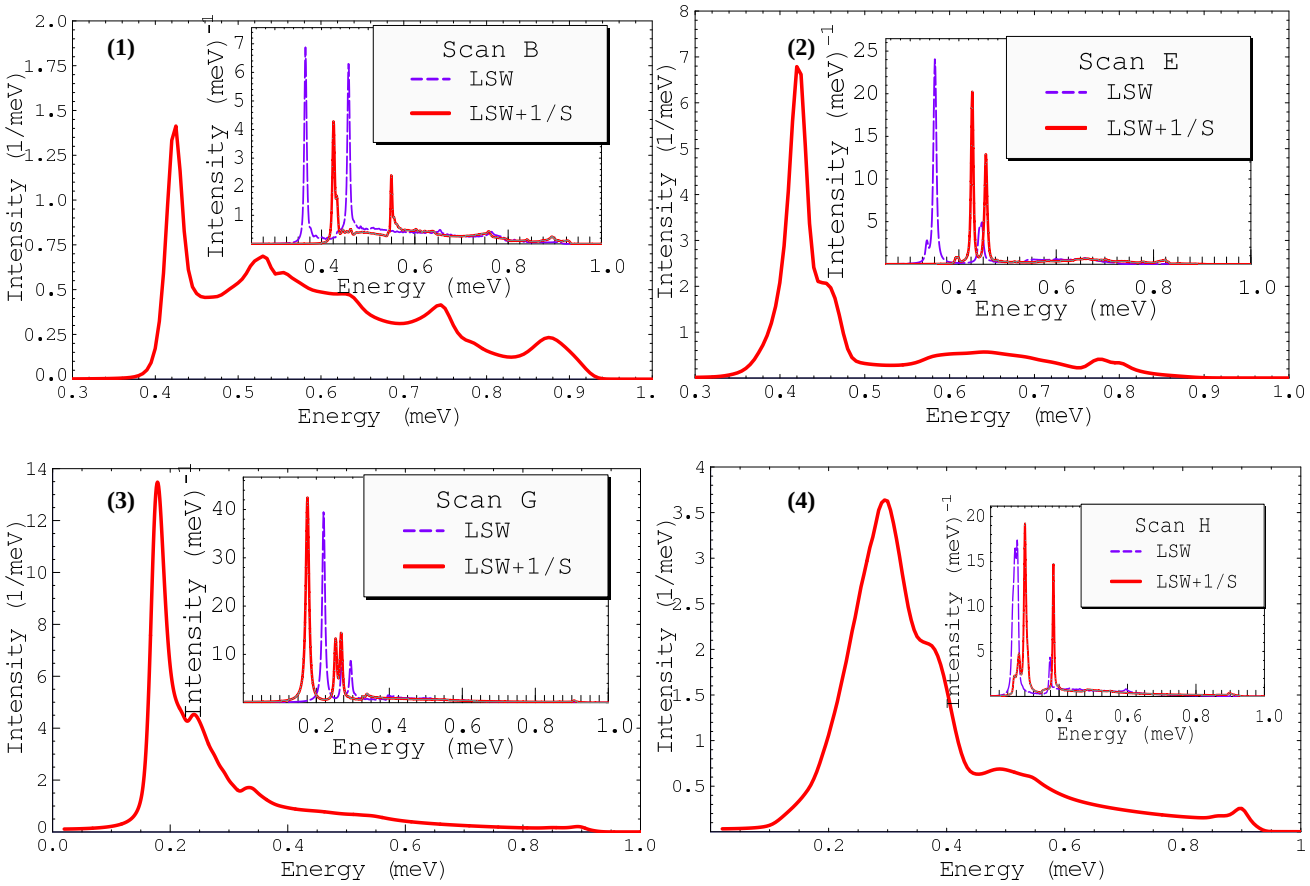


FIG. 9: (Color Online) Scattering cross section. The numbered panels (1-4) correspond to energy scans B, E, G and H respectively. The data has been convolved with the energy and spatial resolution. $\Delta E = 0.016$ meV for all plots and $\Delta k = \{0.035, 0.039, 0.085, 0.056\}$ for plots (1-4). The insets show the results of linear spin wave (LSW) theory and the $1/S$ expansion (LSW+1/S) for $\Delta k = 0, \Delta E = 0.002$ meV.

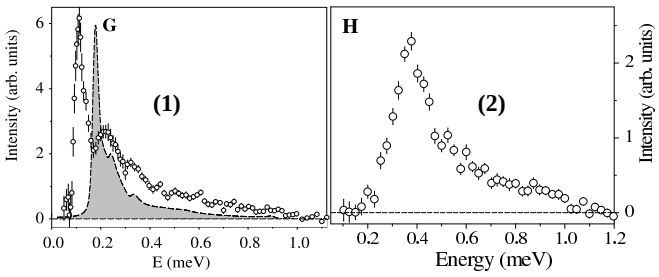


FIG. 10: Observed neutron scattering lineshape in scan G (1) and H (2) (data from Ref. 4) in the ordered phase ($T < 0.1K$). In scan G, the shaded area represents the the 1/S calculation (Eq. (39)) convolved with the experimental resolution.

shifted upwards in energy and carries approximately a quarter of the total spectral weight. Once again the spin wave dispersion is close to a saddle point and as a result the effects of the finite momentum resolution are small. The main feature in the structure factor is a broad peak formed by the two unresolved ω^- and ω^0 modes. This is quite similar to what is observed experimentally (Fig. 5(E) of Ref. 4). It is then tempting to speculate that the experimentally observed single peak is a result of the accidental near degeneracy of the ω^- and ω^0 modes in the vicinity of $\mathbf{k} = (0, -0.25, 1)$. This would explain both the absence of the ω^- peak in the experimental data and the anomalously large intensity of the observed peak.

In Panel 1 of Fig. 9 we plot the dynamical structure factor for scan B near the wave vector $(2, -0.25, 0)$. Here the polarization factor $(\hat{\mathbf{k}}_a)$ in (39) leads to a strong suppression of the out-of-plane fluctuations and the scattering is almost entirely due to the in-plane $\omega^{\pm}$ spin wave modes. The magnon interactions renormalize ω^+ upwards in energy to approximately 0.42 meV, whereas the ω^- mode disappears in the two magnon scattering continuum. A careful analysis shows that the narrow peak at 0.55 meV is not due to a single-particle excitation but is a feature in the two magnon scattering continuum.

The dominant contribution to the dynamical structure factor in scan A in the vicinity of the wave vector $(1.5, -0.3, 0)$ comes from in-plane fluctuations because the polarization factor $\hat{\mathbf{k}}_a$ suppresses out-of plane fluctuations. As can be seen in Fig. 11, the magnon interactions lead to a spectral weight transfer to higher energies. The peaks near 0.8 meV and

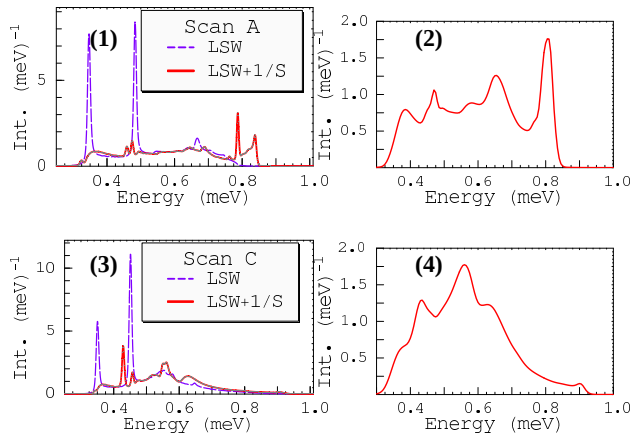


FIG. 11: (Color Online) Calculated scattering cross sections in linear spin wave theory (LSW) and $1/S$ expansion (LSW+$1/S$) for scans A and C. Panels (2) and (4) show the LSW+$1/S$ results with instrumental resolutions of $\Delta E = 0.016$ meV and $\Delta k = 0.02$ (for scan A) and $\Delta k = 0.04$ (for scan C) taken into account. See Fig. 5 from Ref. 4 to compare to experimental data.

0.85 meV can be traced back to single-particle poles in the Green's function. These poles are unphysical and are a result of the uncontrolled nature of the $1/S$ expansion for small values of S. It is easily seen from the Dyson equation (21) that a large self-energy at a given wave vector can lead to "extra" poles in the Green's function at high energies above the two magnon continuum. The inclusion of higher order terms in the $1/S$ expansion would provide decay mechanisms at all energies and lead to a broadening of these high-energy peaks in the dynamical structure factor.

Last but not least let us consider the vicinity of $(0.8, 0.4, 0)$ (scan C). As is shown in Fig. 11 the principal spin wave mode ω^0 is renormalized down to a slightly lower energy of approximately 0.42 meV. The ω^+ mode, which occurs at 0.35 meV in linear spin wave theory, disappears entirely in the two magnon-continuum. The feature near 0.60 meV can again be understood in terms of an enhancement of the two magnon density of states. Comparing with the neutron scattering data (Fig. 5(C) of Ref. 4), the structure factor shows features quite similar to the experimentally observed continuum. However, the scattering continuum occurs at energies nearly 0.10 meV lower than what is observed experimentally.

VI. CONCLUSIONS

In this work we have used nonlinear spin wave theory to determine the dynamical structure factor in the ordered phase of the spin-1/2 helimagnet Cs_2CuCl_4. We have taken into account the first subleading contribution in a $1/S$ expansion, which incorporates interactions between magnons and generates magnon decay processes as well as multi magnon scattering continua. Both effects are particularly pronounced in Cs_2CuCl_4 due to the non-collinear spin ordering, the low spin value and geometrical frustration.

We found that the results of nonlinear spin wave theory explain on a qualitative level many of the features observed in neutron scattering experiments. We find a strong scattering continuum in the dynamical structure factor similar to the experimental observations. Our calculations suggest the possibility that some of the spectral weight at the low-energy boundary of the experimentally observed scattering continuum in scan G could be due to single particle excitations that are unresolved.

In the vicinity of saddle points of the spin wave dispersion relation the single-particle excitations are only weakly affected by the instrumental resolution and hence exhibit sharper peaks in the dynamical structure factor.

In spite of the qualitative agreement of the theory with experiments, crucial discrepancies remain. First and foremost, nonlinear spin wave theory fails to account for the large "quantum renormalization" of the main exchange parameter. This indicates that (to order $\mathcal{O}(S^0)$) the $1/S$ expansion still underestimates the effects of quantum fluctuations. Furthermore, there are significant quantitative differences between our calculations and the experimentally observed structure factor. One may speculate that a better agreement with experiment could be achieved by taking higher-order terms in the $1/S$ expansion into account.

The main lesson to be learned from our calculations is that Cs_2CuCl_4 falls somewhere in between the two theoretical scenarios that have been proposed previously. Our analysis shows that the physics of order plays an essential part in understanding the dynamic response Cs_2CuCl_4 at low temperatures: a large fraction of the spectral weight is carried by spin wave modes, which occur over a large range of frequencies. This is a strong indication that a putative spin-liquid ground state is plainly not a good starting point for the description of the ordered phase of Cs_2CuCl_4. On the other hand we have seen that (in low orders in $1/S$) nonlinear spin wave theory significantly underestimates the effects of quantum fluctuations and hence expansions around the ordered state also fail to account for the experimental observations.

Nonlinear spin wave theory can also be applied to investigate the effects of magnetic fields. It is known that in the presence of a field linear spin wave theory is generally a very poor approximation as it excludes all-important magnon decay processes.[33] A self-consistent study of magnetic field effects in Cs_2CuCl_4 is currently under way.[34] During completion of this work, we became aware of a parallel effort which reaches similar conclusions.[35]

Acknowledgments

The work was supported by the EPSRC under Grant GR/R83712/01. We are grateful to John Chalker and Alan Tennant for valuable discussions. Particular thanks are due to Radu Coldea for numerous helpful discussions and suggestions as well as providing us with figures 8 and 10.

[1] R. Coldea, D. A. Tennant, R. A. Cowley, D. F. McMorrow, B. Dorner, and Z. Tylczynski, Phys. Rev. Lett. **79**, 151 (1997).
[2] R. Coldea, D. A. Tennant, A. M. Tsvelik, and Z. Tylczynski, Phys. Rev. Lett. **86**, 1335 (2001).
[3] R. Coldea, D. A. Tennant, K. Habicht, P. Smeibidl, C. Wolters, and Z. Tylczynski, Phys. Rev. Lett. **88**, 137203 (2002).
[4] R. Coldea, D. A. Tennant, and Z. Tylczynski, Phys. Rev. B **68**, 134424 (2003).
[5] M. Bocquet, F. H. L. Essler, A. M. Tsvelik, and A. O. Gogolin, Phys. Rev. B **64**, 094425 (2001).
[6] M. Bocquet, Phys. Rev. B **65**, 184415 (2002).
[7] C. H. Chung, J. B. Marston, and R. H. McKenzie, J. Phys. : Condens. Matter **13**, 5159 (2001).
[8] S. -Q. Shen and F. C. Zhang, Phys. Rev. B **66**, 172407 (2002).
[9] C. -H. Chung, K. Voelker, and Y. B. Kim, Phys. Rev. B **68**, 094412 (2003).
[10] S. V. Isakov, T. Senthil, and Y. B. Kim, cond-mat/0503241 (unpublished).
[11] J. Y. Gan, F. C. Zhang, and Z. B. Su, Phys. Rev. B **67**, 144427 (2003).
[12] Y. Zhou and X. -G. Wen, cond-mat/0210662 (unpublished).
[13] C. M. Canali and M. Wallin, Phys. Rev. B **48**, R3264 (1993).
[14] C. J. Hamer, Z. Weihong and P. Arndt, Phys. Rev. B **46**, R6276 (1992).
[15] J. I. Igarashi, Phys. Rev. B **46** 10763 (1992).
[16] A. W. Sandvik and R. R. P. Singh, Phys. Rev. Lett. **86**, 528 (2001).
[17] R. R. P. Singh and M. P. Gelfand, Phys. Rev. B **52**, R15695 (1995).
[18] M. P. Gelfand and R. R. P. Singh, Adv. Phys. **49**, 93 (2000).
[19] A. V. Chubukov, S. Sachdev, and T. Senthil, J. Phys: Condens. Matter **6**, 8891 (1994).
[20] T. Nikuni and H. Shiba, J. Phys. Soc. Jpn. **62**, 3268 (1993).
[21] T. Ohyama and H. Shiba, J. Phys. Soc. Jpn. **62**, 3277 (1993).
[22] T. Ohyama and H. Shiba, J. Phys. Soc. Jpn. **63**, 3454 (1994).
[23] I. E. Dzyaloshinsky, J. Phys. Chem. Solids **4**, 241 (1958).
[24] T. Moriya, Phys. Rev. **120**, 91 (1960).
[25] T. Holstein and H. Primakoff, Phys. Rev. **58**, 1098 (1940).
[26] T. Nagamiya, *Solid State Physics*, edited by F. Seitz, D. Turnbull and H. Ehrenreich (Academic, New York, 1967), Vol. 2, p. 305; J. Jensen and A. R. Mackintosh, *Rare Earth Magnetism. Structures and Excitations* (Clarendon, Oxford, 1991), p. 286.
[27] R. M. White, *Quantum Theory of Magnetism* (Springer, Berlin, 1983).
[28] M. E. Zhitomirsky and I. A. Zaliznyak, Phys. Rev. B **53**, 3428 (1996).
[29] M. E. Zhitomirsky and T. Nikuni, Phys. Rev. B **57**, 5013 (1998).
[30] M. Y. Veillette, J. T. Chalker and R. Coldea, cond-mat/0501347 (unpublished).
[31] S. W. Lovesey, *Condensed Matter Physics: Dynamic Correlations*, 2nd ed. (Benjamin/Cummings, New York, 1986), p. 66.
[32] *International Tables for Crystallography*, edited by A. J. C. Wilson, (Kluwer,Dordrecht, 1995), Vol. C, p. 391.
[33] M. E. Zhitomirsky and A. L. Chernyshev, Phys. Rev. Lett. **82**, 4536 (1999).
[34] A. J. A. James, M. Y. Veillette and F. H. L. Essler, in preparation (unpublished).
[35] D. Dalidovich, R. Sknepnek, J. Zhang, C. Kallin, and J. Berlinsky, (unpublished).